



## Discover Generics

Cost-Effective CT & MRI Contrast Agents

 **FRESENIUS  
KABI**

[WATCH VIDEO](#)

# AJNR












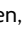









This information is current as  
of June 8, 2025.

## **Different from the Beginning: WM Maturity of Female and Male Extremely Preterm Neonates—A Quantitative MRI Study**

V.U. Schmidbauer, M.S. Yildirim, G.O. Dovjak, K. Goeral,  
J. Buchmayer, M. Weber, M.C. Diogo, V. Giordano, G.  
Mayr-Geisl, F. Prayer, M. Stuempflen, F. Lindenlaub, V.  
List, S. Glatter, A. Rauscher, F. Stuhr, C. Lindner, K.  
Klebermass-Schrehof, A. Berger, D. Prayer and G. Kasprian

*AJNR Am J Neuroradiol* published online 24 March 2022  
<http://www.ajnr.org/content/early/2022/03/24/ajnr.A7472>

# Different from the Beginning: WM Maturity of Female and Male Extremely Preterm Neonates—A Quantitative MRI Study

 V.U. Schmidbauer,  M.S. Yildirim,  G.O. Dovjak,  K. Goeral,  J. Buchmayer,  M. Weber,  M.C. Diogo,  V. Giordano,  G. Mayr-Geisl,  F. Prayer,  M. Stuempflen,  F. Lindenlaub,  V. List,  S. Glatter,  A. Rauscher,  F. Stühr,  C. Lindner,  K. Klebermass-Schrehof,  A. Berger,  D. Prayer, and  G. Kasprian



## ABSTRACT

**BACKGROUND AND PURPOSE:** Former preterm born males are at higher risk for neurodevelopmental disabilities compared with female infants born at the same gestational age. This retrospective study investigated sex-related differences in the maturity of early myelinating brain regions in infants born <28 weeks' gestational age using diffusion tensor- and relaxometry-based MR imaging.

**MATERIALS AND METHODS:** Quantitative MR imaging sequence acquisitions were analyzed in a sample of 35 extremely preterm neonates imaged at term-equivalent ages. Quantitative MR imaging metrics (fractional anisotropy; ADC [ $10^{-3}\text{mm}^2/\text{s}$ ]; and T1-/T2-relaxation times [ms]) of the medulla oblongata, pontine tegmentum, midbrain, and the right/left posterior limbs of the internal capsule were determined on diffusion tensor- and multidynamic, multiecho sequence-based imaging data. ANCOVA and a paired *t* test were used to compare female and male infants and to detect hemispheric developmental asymmetries.

**RESULTS:** Seventeen female (mean gestational age at birth: 26 + 0 [SD, 1 + 4] weeks+days) and 18 male (mean gestational age at birth: 26 + 1 [SD, 1 + 3] weeks+days) infants were enrolled in this study. Significant differences were observed in the T2-relaxation time ( $P = .014$ ) of the pontine tegmentum, T1-relaxation time ( $P = .011$ )/T2-relaxation time ( $P = .024$ ) of the midbrain, and T1-relaxation time ( $P = .032$ ) of the left posterior limb of the internal capsule. In both sexes, fractional anisotropy ( $P [♀] < .001/P [♂] < .001$ ) and ADC ( $P [♀] = .017/P [♂] = .028$ ) differed significantly between the right and left posterior limbs of the internal capsule.

**CONCLUSIONS:** The combined use of various quantitative MR imaging metrics detects sex-related and interhemispheric differences of WM maturity. The brainstem and the left posterior limb of the internal capsule of male preterm neonates are more immature compared with those of female infants at term-equivalent ages. Sex differences in WM maturation need further attention for the personalization of neonatal brain imaging.

**ABBREVIATIONS:** FA = fractional anisotropy; GA = gestational age; ICC = intraclass correlation coefficient; MDME = multidynamic multiecho; PLIC = posterior limb of the internal capsule; PMA = postmenstrual age; T1R = T1-relaxation time; T2R = T2-relaxation time

**B**rain myelination begins prenatally and reaches completion in the third decade of life.<sup>1</sup> The biochemical composition of the myelin sheath causes T1- and T2-weighted MR imaging signal

intensity characteristics, which allow the radiologic evaluation of the human WM maturation.<sup>2-4</sup>


Preterm delivery interferes with regular brain maturation and leads to delays in myelin development.<sup>5</sup> Since prematurity is associated with future neurologic and cognitive impairment,<sup>6-9</sup> the neuroradiologic assessment of brain myelination is paramount to evaluate the risk of potential disabilities in later life. Despite MR imaging being the current standard of reference for neonatal brain imaging, subjective radiologic assessments are limited by the visually subtle effects of small myelin quantities on T1-/T2-weighted MR imaging contrasts.<sup>1,4,5,10</sup> Hence, subtle myelin-related signal intensity changes may escape conventional, qualitative MR imaging evaluations.<sup>5</sup>

Diffusion tensor- and relaxometry-based mapping techniques provide objective, quantitative metrics for cerebral development.<sup>11-13</sup> Recent multidynamic multiecho (MDME) sequence-

Received October 2, 2021; accepted after revision January 25, 2022.

From the Department of Biomedical Imaging and Image-guided Therapy (V.U.S., M.S.Y., G.O.D., M.W., F.P., M.S., F.L., F.S., C.L., D.P., G.K.); Comprehensive Center for Pediatrics (K.G., J.B., V.G., V.L., S.G., K.K.-S., A.B.); Department of Pediatrics and Adolescent Medicine, Division of Neonatology, Pediatric Intensive Care and Neuropediatrics; and Department of Neurosurgery (G.M.-G.), Medical University of Vienna, Vienna, Austria; Department of Neuroradiology (M.C.D.), Hospital Garcia de Orta, Almada, Portugal; and Department of Pediatrics (A.R.), University of British Columbia, Vancouver, British Columbia, Canada.

Please address correspondence to Gregor Kasprian, MD, Department of Biomedical Imaging and Image-guided Therapy, Medical University of Vienna, Waehringer Guertel 18-20, 1090 Vienna, Austria; e-mail: gregor.kasprian@meduniwien.ac.at

 Indicates article with online supplemental data.

<http://dx.doi.org/10.3174/ajnr.A7472>

**Table 1: Demographics and characteristics of included neonates**

	Extremely Preterm Neonates <sup>a</sup> (n = 35)		Unpaired T Test <sup>b</sup> /Fisher Exact Test <sup>c</sup>
	Female (n = 17)	Male (n = 18)	
Neonatal characteristics			
GA at birth (weeks + days) <sup>d</sup>	26 + 0, SD = 1 + 4; R = 23 + 3–27 + 6	26 + 1, SD = 1 + 3; R = 23 + 4–27 + 6	P = .787
Vaginal delivery	n = 3	n = 2	P = .658
Caesarean delivery	n = 14	n = 16	P = .658
Birth weight (g) <sup>d</sup>	773, SD = 250; R = 480–1500	918, SD = 241; R = 530–1300	P = .091
Singleton pregnancy	n = 10	n = 12	P = .733
Multiple pregnancy	n = 7	n = 6	P = .733
Surfactant received	n = 17	n = 18	P > .999
PMA at MR imaging (weeks + days) <sup>d</sup>	37 + 4, SD = 2 + 1; R = 34 + 0–43 + 4	37 + 0, SD = 1 + 2; R = 35 + 1–40 + 2	P = .283
Maternal characteristics			
Maternal age at delivery (yr) <sup>d</sup>	33, SD = 5; R = 22–40	30, SD = 6; R = 19–38	P = .145
Presence of pre-eclampsia	n = 5	n = 2	P = .228
Presence of GDM	n = 1	n = 0	P = .486
Presence of IAI <sup>e</sup>	n = 2	n = 2	P > .999
Neonatal mortality risk			
CRIB II scored <sup>d</sup>	11, SD = 2; R = 7–16	11, SD = 3; R = 8–17	P = .928
Neonatal diagnoses <sup>f</sup>			
Perinatal asphyxia <sup>g</sup>	n = 4	n = 6	P = .711
Patent ductus arteriosus	n = 3	n = 0	P = .104
Necrotizing enterocolitis	n = 1	n = 1	P > .999
Bronchopulmonary dysplasia	n = 3	n = 3	P > .999
Retinopathy of prematurity	n = 9	n = 7	P = .505

**Note:**—CRIB II indicates Clinical Risk Index for Babies II; GDM, gestational diabetes mellitus; IAI, intra-amniotic infection (chorioamnionitis).

<sup>a</sup>Born before 28 weeks' gestation (routine MR imaging of the preterm neonatal brain at approximately term-equivalent age).

<sup>b</sup>Applies to metric data.

<sup>c</sup>Applies to categoric variables.

<sup>d</sup>Data presented as mean (SD) and range (R).

<sup>e</sup>Based on clinical presentation, placental histology, bacterial culture, and blood markers of inflammation.

<sup>f</sup>Neonates could be represented in multiple rows (>1 condition).

<sup>g</sup>Based on clinical presentation, Apgar scores, umbilical cord pH, and first blood gas analysis (pH, base excess, and lactate) (absence of asphyxia-induced brain injury).

acquisition strategies provide a variety of MR imaging contrasts and quantitative maps based on a single scan of <6 minutes.<sup>14–16</sup> Therefore, SyMRI-based (SyntheticMR) MDME postprocessing (postprocessing time, <1 minute) makes tissue-specific T1-/T2-relaxation time (T1R/T2R) metrics available in a clinically acceptable time.<sup>16</sup> The capability to quantify myelination in the neonatal brain using diffusion tensor parameters (fractional anisotropy [FA] and ADC) and relaxation properties (T1R and T2R) has been demonstrated in previous investigations.<sup>12,17</sup>

Sex and gestational age (GA) at birth have an impact on WM maturation and on the neurodevelopmental outcome of former preterm neonates.<sup>5,8,17,18</sup> Evidence suggests that male infants born before 28 weeks' gestation are at the highest risk of severe cognitive impairment.<sup>8,9,18,19</sup> This investigation was conducted to prove that prematurity affects brain maturation differently in females and males at early developmental stages. Thus, diffusion tensor- and relaxometry-based mapping approaches were applied to detect sex-related maturity differences of early myelinating brain regions in a sample of former extremely preterm neonates. In addition, quantitative imaging markers were used to assess hemispheric asymmetries in brain development in both female and male infants. Relationships between diffusion tensor parameters and tissue-specific relaxation time metrics with regard to brain myelination processes were elucidated.

## MATERIALS AND METHODS

### Ethics Approval

The local ethics commission approved the protocol of this retrospective study. All parents/guardians provided written, informed consent for neonatal MR imaging before scanning and agreed to the scientific use of the data.

### Study Sample

Between June 2017 and August 2020, brain MR imaging was performed in 73 extremely preterm infants (GA at birth: <28 + 0 [weeks + days]) at the Department of Neuroradiology of a tertiary care hospital. All infants were referred for neuroimaging by the Department of Neonatology of the same hospital. At Vienna General Hospital, Medical University of Vienna, brain MR imaging (imaging at approximately term-equivalent age) is performed routinely in former extremely preterm infants. After a review of the imaging data by 1 neonatal neuroimaging expert with 15 years' experience, all neonates with brain scans with pathologic findings were excluded from this study. Thus, only infants without intracranial pathologic brain imaging findings were included (Table 1). At the time of imaging, none of the included infants presented with neurologic symptoms.

### Neonatal MR Imaging, Quantitative Sequence, and MR Imaging Data Postprocessing

Before MR imaging, infants were fed or slightly sedated (chloral hydrate, 30–50 mg/kg, or chloral hydrate, 30 mg/kg, combined

**Table 2: Quantitative MR imaging sequences**

	MDME	DTI
TR (ms)	3309	2435
TE (ms)	13; 100	88
Acquired voxel size (mm)	$0.89 \times 1.04 \times 4.00$	$2.41 \times 2.48 \times 2.50$
FOV (mm)	$200 \times 165 \times 109$	$164 \times 164 \times 100$
Echo-train <sup>a</sup> /EPI factor <sup>b</sup>	10	33
Pixel/Hz	1366/159.0	5310/40.9
Sense factor	2	2
Gap (mm)	1	0
Slice number	22	40
b-value (s/mm <sup>2</sup> )		0/800
Directional resolution		32
Acquisition time (min)	05:24	05:26

**Note:**—MDME indicates multidynamic multiecho.

<sup>a</sup> Applies to MDME sequence.

<sup>b</sup> Applies to diffusion tensor imaging sequence.

with midazolam, 0.1 mg/kg) and bedded in a vacuum mattress. All neonates were imaged using a standardized neonatal MR imaging protocol (Online Supplemental Data) on an Ingenia (Philips Healthcare) 1.5T MR imaging system equipped with a 32-channel head coil. An axial MDME sequence and an axial diffusion tensor imaging sequence (flip angle = 90°) (Table 2) were acquired to obtain quantitative data. By applying 2 repeated acquisition phases (phase 1: saturation of 1 section by a section-selective saturation pulse [flip angle = 120°]; and phase 2: generation of a series of spin echoes for another section by section-selective excitation pulses [flip angle = 90°] and section-selective refocusing pulses [flip angle = 180°]), the MDME sequence acquires information about T1R/T2R parameters of the investigated tissue.<sup>16,20,21</sup> The MDME sequence postprocessing software SyMRI (Version 11.2) was used to generate quantitative T1R-/T2R-based maps. Diffusion tensor data were postprocessed using the IntelliSpace Portal (Version 10; Philips Healthcare).

### Determination of Quantitative Parameters

Diffusion tensor parameters (FA; ADC [ $10^{-3}$  mm<sup>2</sup>/s]) and tissue-specific relaxation time metrics (T1R [ms]; T2R [ms]) were quantified in infratentorial and supratentorial neonatal brain regions, which are characterized by advanced states of myelination.<sup>1</sup> ROI placement was performed manually on diffusion tensor-based data and SyMRI-generated maps (Fig 1) by 2 different raters (rater 1, with 3 years' experience and rater 2, with 2 years' experience with neonatal neuroimaging). To ensure maximal overlap across diffusion tensor and relaxation time measures, we conducted a multisection approach. Therefore, for each brain section of interest, 2 separate ROIs were drawn at different levels (performed by both raters in a consensus reading): medulla oblongata (ROI 1: level of the inferior olive; ROI 2: level of the dorsal column nuclei); pontine tegmentum (ROI 1: level of the locus coeruleus; ROI 2: level of the superior olive); midbrain (ROI 1: level of the superior colliculus/intercollicular area; ROI 2: level of the inferior colliculus); and right/left posterior limbs of the internal capsule (PLICs) (ROI 1: level of the foramen of Monro; ROI 2: level of the third ventricle). On the basis of both ROI drawings for each section, the mean values of FA, ADC, T1R, and T2R were calculated. If the implementation of a multisection approach

was not possible (ie, multiple contiguous slices were not provided, poor delineability of ROIs), 2 separate measures were obtained on 1 appropriate section.

### Statistical Analysis

Two groups were defined for statistical analyses: female and male neonates. SPSS Statistics for Macintosh (Version 25.0; IBM) was used for statistical analyses at a significance level of  $\alpha = 5\%$  ( $P < .05$ ). Metric data are expressed as means (SD). To summarize the overall agreement of the quantitative parameters determined by both raters, we calculated an intraclass correlation coefficient (ICC) for each ROI. ICC values  $\geq 0.75$  were considered strong agreement.<sup>22</sup> In case of strong concordances, the results of rater 1 were presented. If there were no strong concordances, the results of both raters were reported. To detect differences in FA, ADC, T1R, and T2R of the medulla oblongata, pontine tegmentum, midbrain, right PLIC, and left PLIC between the groups, we performed an ANCOVA. GA at birth; mode of delivery; birth weight; singleton/multiple pregnancy; receipt of surfactant; postmenstrual age (PMA) at MR imaging; maternal age at delivery; presence of pre-eclampsia, gestational diabetes, and chorioamnionitis; Clinical Risk Index for Babies II score;<sup>23</sup> and neonatal diagnoses (Table 1) were defined as covariates to correct for possible confounding effects. An unpaired *t* test (metric data) and a Fisher exact test (categorical variables) were used to detect between-group differences in these variables (Table 1). A paired *t* test was used to assess differences in FA, ADC, T1R, and T2R between the right and left PLICs in both female and male infants. Within both groups, a Pearson correlation analysis was performed to detect relationships between FA and T1R, FA and T2R, ADC and T1R, and ADC and T2R. Multiple-comparison correction was waived due to the small sample size and the increased risk of type II error.<sup>24</sup>

### RESULTS

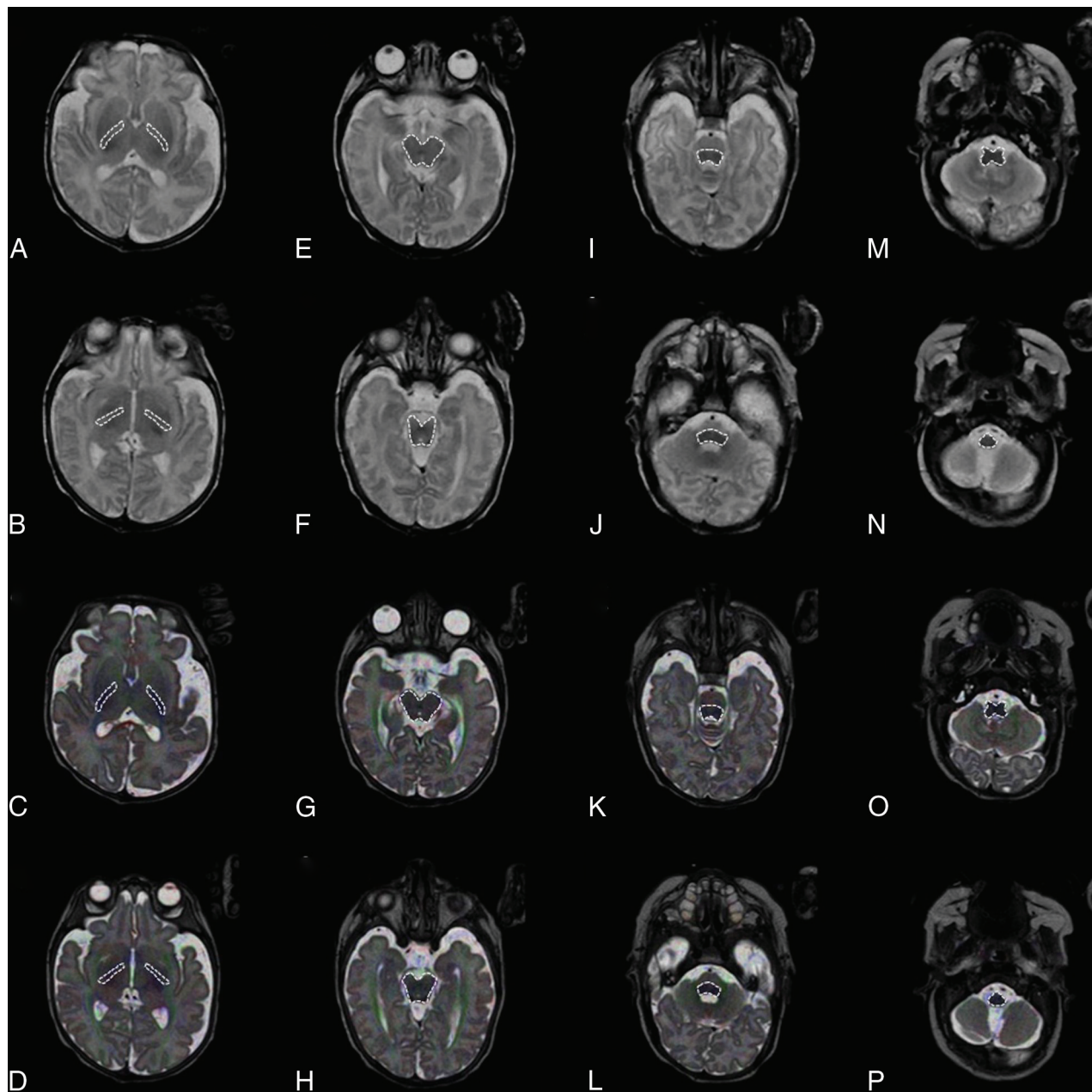
A total of 35/73 (48%) neonates (female:  $n = 17$ ; mean GA at birth:  $26 \pm 0$  [SD, 1 + 4] weeks+days; mean PMA at MR imaging:  $37 \pm 4$  [SD, 2 + 1] weeks+days; male:  $n = 18$ , mean GA at birth:  $26 \pm 1$  [SD, 1 + 3] weeks+days; mean PMA at MR imaging:  $37 \pm 0$  [SD, 1 + 2] weeks+days) were included in this study (Table 1). The remaining 38/73 (52%) infants were not enrolled due to pathologic brain MR imaging findings (hemorrhage,  $n = 35$ ; periventricular leukomalacia,  $n = 2$ ; and arteriovenous malformation,  $n = 1$ ).

### ICC Analysis

For relaxation time metrics, ICC values ranged between 0.831 (95% CI, 0.249–0.948) and 0.986 (95% CI, 0.962–0.995).

For diffusion tensor parameters, ICC values ranged between 0.604 (95% CI, –0.001–0.852) and 0.994 (95% CI, 0.982–0.998). There were no strong correlations between the ADC values determined by both raters in the right/left PLICs (0.743; 95% CI, 0.270–0.908; 0.604; 95% CI, –0.001–0.852) of females and in the medulla oblongata (0.713; 95% CI, 0.068–0.902) and the pontine tegmentum (0.605; 95% CI, –0.038–0.851) of male preterm neonates (Online Supplemental Data).





**FIG 1.** ROI placement is demonstrated on an SymMRI-generated T2-weighted MR imaging contrast (A, B, E, F, I, J, M, N) (TR = 4500 ms; TE = 100 ms; axial plane) and a diffusion tensor map superimposed on a T2-weighted turbo spin-echo sequence-based image (C, D, G, H, K, L, O, P) (TR = 3000 ms; TE = 140 ms; axial plane) of a female infant (GA at birth: 24 + 4 weeks + days; PMA at MR imaging: 39 + 2 weeks + days). For each investigated brain region, 2 separate ROIs were defined at different levels: right/left PLIC (ROI 1: level of the foramen of Monro [A and C]; ROI 2: level of the third ventricle [B and D]); midbrain (ROI 1: level of the superior colliculus/intercollicular area [E and G]; ROI 2: level of the inferior colliculus [F and H]); pontine tegmentum (ROI 1: level of the locus coeruleus [I and K]; ROI 2: level of the superior olive [J and L]); and medulla oblongata (ROI 1: level of the inferior olive [M and O]; ROI 2: level of the dorsal column nuclei [N and P]).

### Differences between Female and Male Neonates

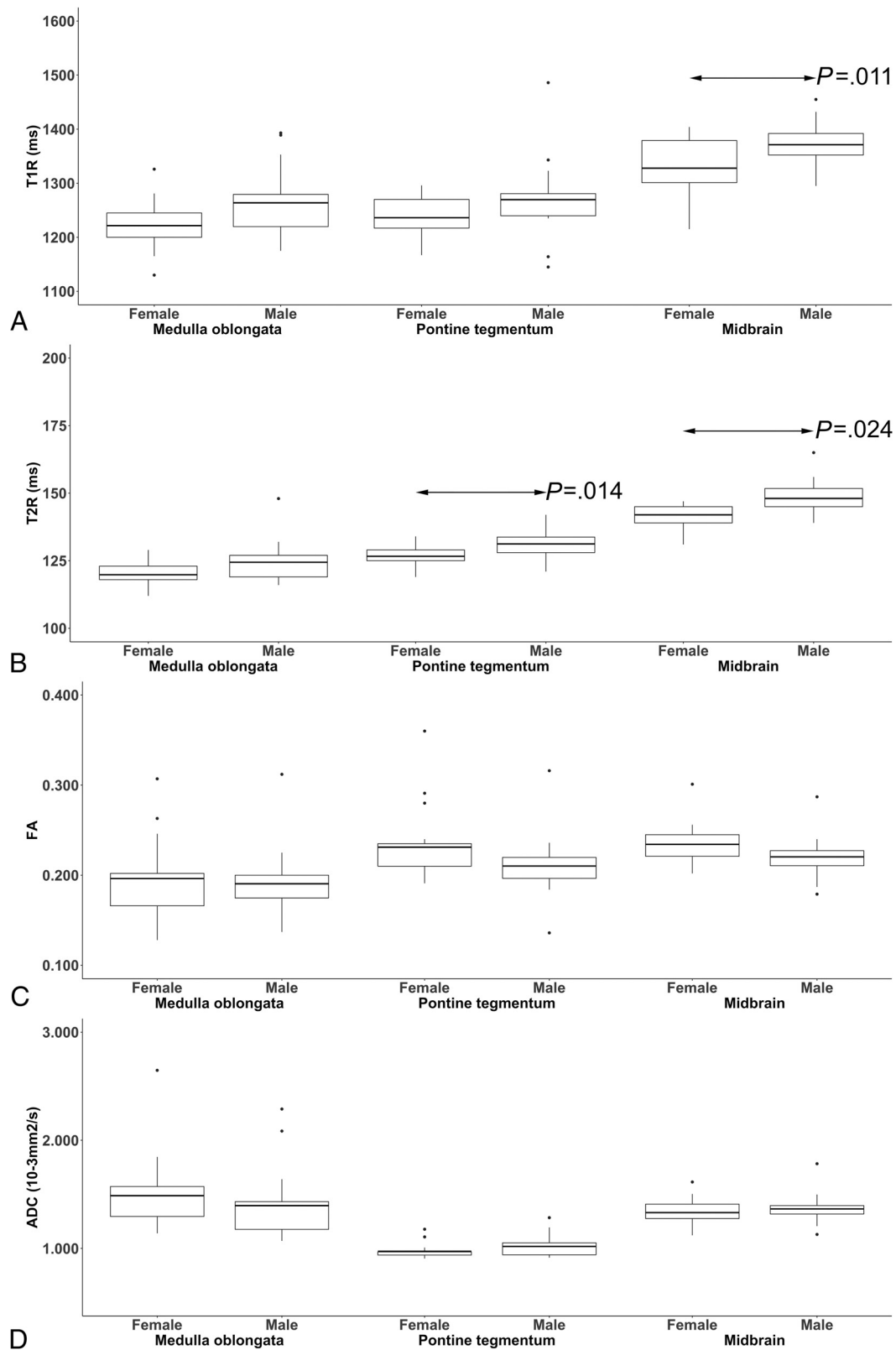
Significant differences between female and male infants were observed in T2R ( $P = .014$ ) of the pontine tegmentum, T1R ( $P = .011$ ) and T2R ( $P = .024$ ) of the midbrain, and T1R ( $P = .032$ ) of the left PLIC.

Based on FA ( $P = .529$ ), ADC (rater 1:  $P = .651$ ; rater 2:  $P = .844$ ), T1R ( $P = .073$ ) or T2R ( $P = .099$ ) of the medulla oblongata; FA ( $P = .464$ ), ADC (rater 1:  $P = .100$ ; rater 2:  $P = .581$ ), or T1R ( $P = .124$ ) of the pontine tegmentum; FA ( $P = .200$ ) or ADC ( $P =$

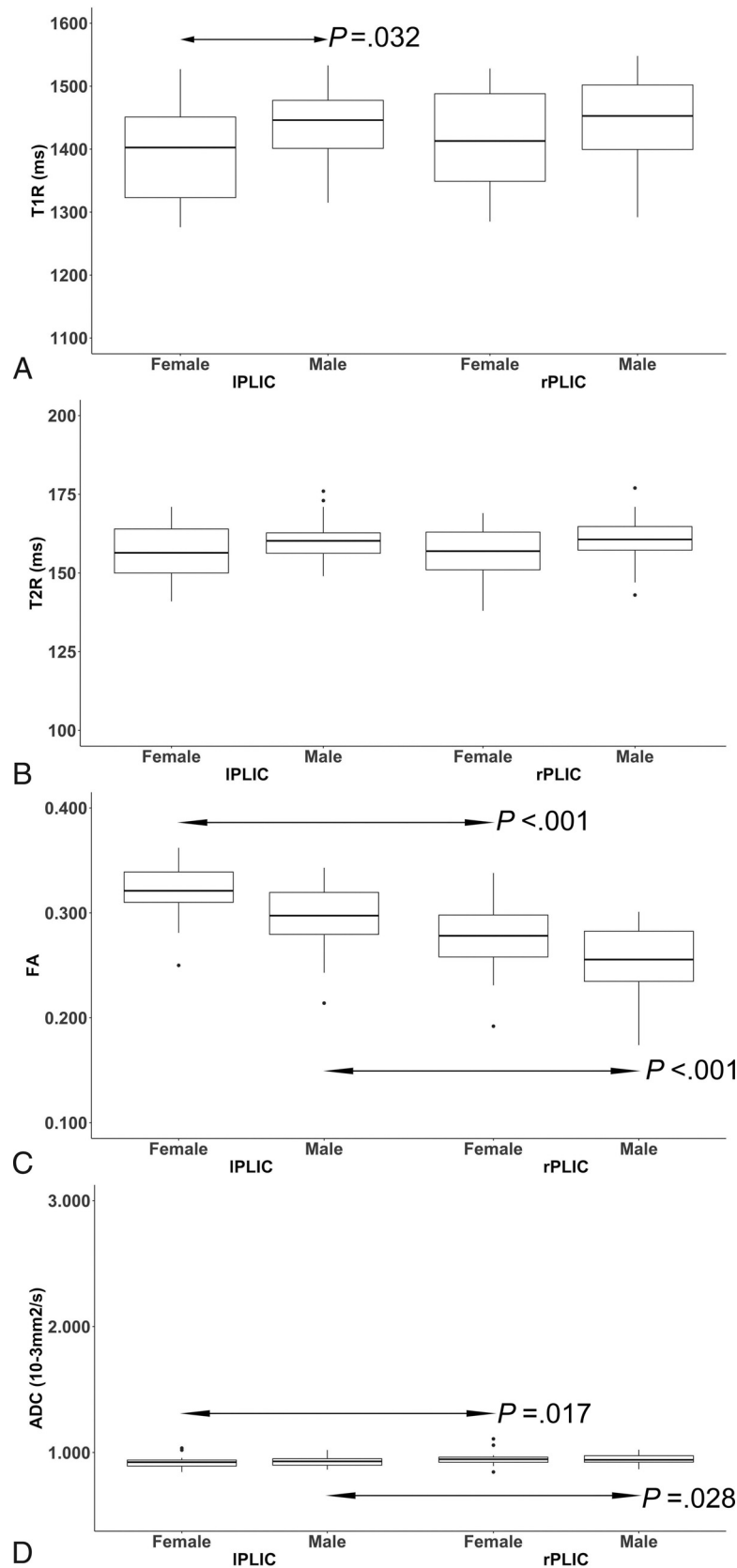
$.828$ ) of the midbrain; FA ( $P = .167$ ), ADC (rater 1:  $P = .809$ ; rater 2:  $P = .675$ ), T1R ( $P = .073$ ), or T2R ( $P = .226$ ) of the right PLIC; and FA ( $P = .244$ ), ADC (rater 1:  $P = .511$ ; rater 2:  $P = .072$ ), or T2R ( $P = .443$ ) of the left PLIC, no significant differences were observed between female and male infants (Figs 2 and 3).

### Hemispheric Asymmetries of the PLIC

**Female Neonates.** There were significant differences in FA ( $P < .001$ ) and ADC (rater 1:  $P = .017$ ; rater 2:  $P < .001$ ) of the



**FIG 2.** The boxplots show sex-related differences in T1-/T2-relaxation time metrics (ms) (A and B) and diffusion tensor parameters (FA; ADC [ $10^{-3}\text{mm}^2/\text{s}$ ]) (C and D) (determined by rater 1 at term-equivalent ages) of the neonatal medulla oblongata, pontine tegmentum, and midbrain. The black bar indicates mean values. Significant differences (arrows) were observed in T1R ( $P=.011$ ) of the midbrain (A), T2R ( $P=.014$ ) of the pontine tegmentum, and T2R ( $P=.024$ ) of the midbrain (B) between female and male neonates.



**FIG 3.** The boxplots show differences in T1/T2-relaxation time metrics (ms) (A and B) and diffusion tensor parameters (FA; ADC [ $10^{-3} \text{mm}^2/\text{s}$ ]) (C and D) (determined by rater 1 at term-equivalent ages) between both sexes and the right/left posterior limbs of the internal capsule (rPLIC/IPLIC). The black bar indicates mean values. Significant sex-related differences (arrow) were observed in T1R ( $P = .032$ ) of the IPLIC (A). In both sexes, FA ( $P [\text{♀}] < .001/P [\text{♂}] < .001$ ) and ADC ( $P [\text{♀}] = .017; P [\text{♂}] = .028$ ) differed significantly (arrows) between the rPLIC and IPLIC (C and D).

left compared with the right PLIC, characterized by higher FA values and lower ADC values (left PLIC). The T1R ( $P = .140$ ) and T2R metrics ( $P = .563$ ) did not reveal significant differences between the right and left PLICs.

**Male Neonates.** There were significant differences in FA ( $P < .001$ ) and ADC ( $P = .028$ ) of the left compared with the right PLIC, characterized by higher FA values and lower ADC values (left PLIC). The T1R ( $P = .162$ ) and T2R metrics ( $P = .740$ ) did not reveal significant differences between the right and left PLICs (Fig 3).

### **Relationships between Diffusion Tensor and Relaxation Time Metrics**

In female infants, there were significant correlations between the ADC and T1R values in the medulla oblongata ( $r = -0.507$ ,  $P = .038$ ) and the midbrain ( $r = -0.516$ ,  $P = .034$ ).

In male infants, there were significant correlations between the ADC and T2R values in the right ( $r = 0.484$ ,  $P = .042$ ) and left PLICs ( $r = 0.492$ ,  $P = .038$ ) (Online Supplemental Data).

## **DISCUSSION**

This study investigated sex-related brain maturity differences at an early stage of development using quantitative MR imaging. Relaxometry-based mapping revealed a more advanced state of brainstem maturation in female compared with male extremely preterm infants at term-equivalent ages. Moreover, on the basis of T1R, myelination appeared more advanced in the left PLIC in females compared with males. Furthermore, diffusion tensor-based metrics detected advanced maturational stages of the left-sided compared with the right-sided internal capsule regions. However, diffusion tensor and relaxation parameters did not show consistent relationships, which might indicate that both modalities respond to different molecular aspects of myelinogenesis. Therefore, the combined use of diffusion tensor- and relaxation property-derived metrics detects subtle characteristics of WM maturation.

Before 30 weeks' GA, brainstem structures (brachium conjunctivum, medial longitudinal fascicle, medial lemniscus, central tegmental tract, and statoacoustic system) already show remarkable myelination, whereas the PLIC has maximum quantities of myelin supratentorially.<sup>1,25</sup> The T1R decreases as premyelination processes occur.<sup>26-28</sup> These are characterized by interactions between isolated myelin components and H<sub>2</sub>O molecules.<sup>26-28</sup> In the course of myelinogenesis, the entry of organic compounds into the myelin sheath results in further T1R shortening.<sup>1</sup> A study in an animal model proved that female sex hormones stimulate the anchoring of proteins into the myelin bilayer.<sup>29</sup> Thus, estrogen and progesterone appear to promote myelin formation. Based on T2R, there were significant differences between both sexes at the level of the pontine tegmentum and the midbrain. As opposed to T1R, T2R shortening occurs as fully developed myelin sheaths progressively tighten.<sup>26-28</sup> Because brain myelination progresses caudally to rostrally, pronounced T2 shortening in the female brainstem appears credible, while maturity-related effects on T2R may have remained limited in supratentorial regions.<sup>1</sup> Although diffusion-based MR imaging has been proved to

visualize gonadal hormone-related maturity differences in WM in an animal model, the quantitative approach applied in this study did not reveal significant results.<sup>30</sup> Although ADC values decrease at the stage of premyelination,<sup>31,32</sup> this parameter seems insensitive to sex-related maturity differences. In contrast to ADC metrics, the FA responds to advanced states of myelin development,<sup>32</sup> possibly explaining the limited ability to detect reliable maturity differences between female and male preterm infants.

On the basis of diffusion tensor metrics, myelination appears more advanced in the left compared with the right PLIC in both sexes. This finding is in keeping with descriptions in the literature.<sup>28</sup> Using diffusion tensor imaging, Dubois et al<sup>28,33</sup> demonstrated left-right asymmetries in the infant brain in favor of left-sided projection tracts. Because somatosensory pathways develop rapidly, extensive myelination is detectable in the PLIC at the beginning of the third trimester of pregnancy, while fully developed myelin sheaths are not detectable before 44 weeks' postconceptional age.<sup>25,33,34</sup> This fact could explain the absence of considerable T2R shortening in the investigated sample. However, even though sex-related differences were observed in T1R of left-sided internal capsule regions, relaxometry-based mapping seems insensitive to hemispheric asynchronies of neonatal brain development.

Diffusion tensor and relaxation time metrics appear to characterize various aspects of myelin maturation: The T1R responds immediately to chemical bonding between H<sub>2</sub>O molecules and myelin building blocks; the increase in membrane attenuation (ADC) and the process of axonal myelin ensheathment (FA) further result in the response of diffusion tensor parameters, whereas tightening of myelin sheaths is required for T2R shortening to occur.<sup>26,31,35</sup> These assumptions are supported by the presented data, which show that diffusion tensor and relaxation time metrics are inconsistently associated.

Preterm delivery accounts for delays in myelin development.<sup>6,7</sup> Our data suggest that brain myelination processes are more severely affected in former extremely preterm males than their female counterparts. The combined use of different, quantitative MR imaging modalities allows sex-related and hemispheric maturity differences to be identified noninvasively at an early stage of development. Quantitative MR imaging might enable physicians to identify infants in need of intensified support and closer follow-up at an early maturational stage and, therefore, increase their chance of favorable neurodevelopmental outcomes. However, this possibility was beyond the scope of the present investigation and needs to be addressed in the future.

This study has several limitations. Quantitative imaging markers were determined only in a limited number of brain regions. However, the investigation of sex-related characteristics of premyelinating areas was beyond the scope of this investigation. Diffusion tensor- and MDME-based imaging data differed in voxel size and section thickness. Therefore, diffusion tensor and relaxation time metrics were potentially determined on different slices. Thus, a multisection approach was conducted to ensure maximal overlap across FA/ADC and T1R/T2R measures. Even though neonates with brain scans with pathologic findings



were excluded, there were still infants with (extracranial) conditions that might impact neurodevelopment. Thus, statistical methods were applied that correct for possible confounding effects of these conditions. This study did not elaborate on the future outcomes of the preterm infants included. Nonetheless, further investigations that link developmental asynchronies/sex-related differences to the lateralization of brain functions are of highest interest. Although only homogeneous cohorts of former preterm born females and males were included in this study, the investigated sample size was small. However, our data revealed considerable sex-related maturity differences at an early stage of human brain development. Nonetheless, sex-related neurodevelopmental differences require further investigation in larger samples.

## CONCLUSIONS

The combined use of diffusion tensor- and relaxometry-based mapping approaches reveals sex-related maturity differences and hemispheric asynchronies of WM maturation. Quantitative imaging markers can detect subtle characteristics of the sequential process of myelination noninvasively at an early stage of cerebral development.

**Disclosure forms** provided by the authors are available with the full text and PDF of this article at [www.ajnr.org](http://www.ajnr.org).

## REFERENCES

- van der Knaap MS, Valk J. *Magnetic Resonance of Myelination and Myelin Disorders*. 3rd ed. Springer-Verlag; 2005
- Barkovich AJ, Kjos BO, Jackson DE, et al. Normal maturation of the neonatal and infant brain: MR imaging at 1.5 T. *Radiology* 1988;166:173–80 [CrossRef Medline](#)
- van der Knaap MS, Valk J. MR imaging of the various stages of normal myelination during the first year of life. *Neuroradiology* 1990;31:459–70 [CrossRef Medline](#)
- Porto L, Kieslich M, Yan B, et al. Accelerated myelination associated with venous congestion. *Eur Radiol* 2006;16:922–26 [CrossRef Medline](#)
- Schmidbauer V, Geisl G, Diogo M, et al. SyMRI detects delayed myelination in preterm neonates. *Eur Radiol* 2019;29:7063–72 [CrossRef Medline](#)
- Ibrahim J, Mir I, Chalakh L. Brain imaging in preterm infants <32 weeks' gestation: a clinical review and algorithm for the use of cranial ultrasound and qualitative brain MRI. *Pediatr Res* 2018;84:799–806 [CrossRef Medline](#)
- Parikh NA. Advanced neuroimaging and its role in predicting neurodevelopmental outcomes in very preterm infants. *Semin Perinatol* 2016;40:530–41 [CrossRef Medline](#)
- Glass HC, Costantino AT, Stayer SA, et al. Outcomes for extremely premature infants. *Anesth Analg* 2015;120:1337–51 [CrossRef Medline](#)
- Marlow N, Wolke D, Bracewell MA, et al; EPICure Study Group. Neurologic and developmental disability at six years of age after extremely preterm birth. *N Engl J Med* 2005;352:9–19 [CrossRef Medline](#)
- Schmidbauer V, Geisl G, Cardoso Diogo M, et al. Validity of SyMRI for assessment of the neonatal brain. *Clin Neuroradiol* 2021;31:315–23 [CrossRef Medline](#)
- Wimberger DM, Roberts TP, Barkovich AJ, et al. Identification of "premyelination" by diffusion-weighted MRI. *J Comput Assist Tomogr* 1995;19:28–33 [CrossRef Medline](#)
- Qiu A, Mori S, Miller MI. Diffusion tensor imaging for understanding brain development in early life. *Annu Rev Psychol* 2015;66:853–76 [CrossRef Medline](#)
- Lee SM, Choi YH, You SK, et al. Age-related changes in tissue value properties in children: simultaneous quantification of relaxation times and proton density using synthetic magnetic resonance imaging. *Invest Radiol* 2018;53:236–45 [CrossRef Medline](#)
- McAllister A, Leach J, West H, et al. Quantitative synthetic MRI in children: normative intracranial tissue segmentation values during development. *AJNR Am J Neuroradiol* 2017;38:2364–72 [CrossRef Medline](#)
- Tanenbaum LN, Tsiouris AJ, Johnson AN, et al. Synthetic MRI for clinical neuroimaging: results of the Magnetic Resonance Image Compilation (MAGiC) prospective, multicenter, multi-reader trial. *AJNR Am J Neuroradiol* 2017;38:1103–10 [CrossRef Medline](#)
- Warntjes JB, Leinhard OD, West J, et al. Rapid magnetic resonance quantification on the brain: optimization for clinical usage. *Magn Reson Med* 2008;60:320–29 [CrossRef Medline](#)
- Schmidbauer V, Dovjak G, Geisl G, et al. Impact of prematurity on the tissue properties of the neonatal brain stem: a quantitative MR approach. *AJNR Am J Neuroradiol* 2021;42:581–89 [CrossRef Medline](#)
- Skiöld B, Alexandrou G, Padilla N, et al. Sex differences in outcome and associations with neonatal brain morphology in extremely preterm children. *J Pediatr* 2014;164:1012–18 [CrossRef Medline](#)
- O'Driscoll DN, McGovern M, Greene CM, et al. Gender disparities in preterm neonatal outcomes. *Acta Paediatr* 2018;107:1494–99 [CrossRef](#)
- Hagiwara A, Warntjes M, Hori M, et al. SyMRI of the brain: rapid quantification of relaxation rates and proton density, with synthetic MRI, automatic brain segmentation, and myelin measurement. *Invest Radiol* 2017;52:647–57 [CrossRef Medline](#)
- Kang KM, Choi SH, Kim H, et al. The effect of varying slice thickness and interslice gap on T1 and T2 measured with the multidynamic multiecho sequence. *Mag Reson Med Sci* 2019;18:126–33 [CrossRef Medline](#)
- Cicchetti D. Guidelines, criteria, and rules of thumb for evaluating normed and standardized assessment instruments in psychology. *Psychol Assess* 1994;6:284–90 [CrossRef](#)
- Bührer C, Metze B, Obladen M. CRIB, CRIB-II, birth weight or gestational age to assess mortality risk in very low birth weight infants? *Acta Paediatr* 2008;97:899–903 [CrossRef Medline](#)
- Rothman KJ. No adjustments are needed for multiple comparisons. *Epidemiology* 1990;1:43–46 [CrossRef Medline](#)
- Yakovlev P, Lecours A. The myelogenetic cycles of regional maturation of the brain. In: Minkowski A, eds. *Regional Development of the Brain in Early Life*. Oxford: Blackwell; 1967; 3–70
- Wang S, Ledig C, Hajnal JV, et al. Quantitative assessment of myelination patterns in preterm neonates using T2-weighted MRI. *Sci Rep* 2019;9:12938 [CrossRef Medline](#)
- Barkovich AJ, Lyon G, Evrard P. Formation, maturation, and disorders of white matter. *AJNR Am J Neuroradiol* 1992;13:447–61 [Medline](#)
- Dubois J, Dehaene-Lambertz G, Kulikova S, et al. The early development of brain white matter: a review of imaging studies in fetuses, newborns and infants. *Neuroscience* 2014;276:48–71 [CrossRef Medline](#)
- Darling JS, Daniel JM. Pubertal hormones mediate sex differences in levels of myelin basic protein in the orbitofrontal cortex of adult rats. *Neuroscience* 2019;406:487–95 [CrossRef Medline](#)
- Prayer D, Roberts T, Barkovich AJ, et al. Diffusion-weighted MRI of myelination in the rat brain following treatment with gonadal hormones. *Neuroradiology* 1997;39:320–25 [CrossRef Medline](#)
- Dubois J, Dehaene-Lambertz G, Perrin M, et al. Asynchrony of the early maturation of white matter bundles in healthy infants:

- quantitative landmarks revealed noninvasively by diffusion tensor imaging. *Hum Brain Mapp* 2008;29:14–27 [CrossRef](#) [Medline](#)
32. Woitek R, Prayer D, Weber M, et al. Fetal diffusion tensor quantification of brainstem pathology in Chiari II malformation. *Eur Radiol* 2016;26:1274–83 [CrossRef](#) [Medline](#)
33. Dubois J, Hertz-Pannier L, Cachia A, et al. Structural asymmetries in the infant language and sensori-motor networks. *Cereb Cortex* 2009;19:414–23 [CrossRef](#) [Medline](#)
34. Kinney HC, Brody BA, Kloman AS, et al. Sequence of central nervous system myelination in human infancy, II: patterns of myelination in autopsied infants. *J Neuropathol Exp Neurol* 1988;47:217–34 [CrossRef](#) [Medline](#)
35. Uddin MN, Figley TD, Solar KG, et al. Comparisons between multi-component myelin water fraction, T1w/T2w ratio, and diffusion tensor imaging measures in healthy human brain structures. *Sci Rep* 2019;9:2500 [CrossRef](#) [Medline](#)